Research Square

Preprints are preliminary reports that have not undergone peer review.
They should not be considered conclusive, used to inform clinical practice,
or referenced by the media as validated information.

ERK hyperactivation drives myelin repair and functional recovery via direct Olig2 targeting

Jialin Li
Fudan University
Feihong Yang
Fudan University
Wenhui Zheng
Fudan University
Danyu Han
Fudan University
Zizhuo Sha
Fudan University
Dashi Qi
Fudan University
Zhuangzhi Zhang
zz_zhang@fudan.edu.cn
Fudan University
Jing Ding
Fudan University
Xin Wang
Fudan University

Research Article

Keywords: multiple sclerosis, remyelination, oligodendrocyte precursor cells, MAPK/ERK signaling, Olig2

Posted Date: November 23rd, 2026

DOI: https://doi.org/10.21203/rs.3.rs-11754770/v1

License: This work is licensed under a Creative Commons Attribution 4.0 International License.
Read Full License

Additional Declarations: No competing interests reported.

ERK hyperactivation drives myelin repair and functional recovery via direct *Olig2* targeting

Jialin Li[1]†, Feihong Yang[2]†, Wenhui Zheng[1], Danyu Han[1], Zizhuo Sha[1], Dashi Qi[1], Zhuangzhi Zhang*[1], Jing Ding*[1], Xin Wang*[1]

†These authors contributed equally to this work

[1]Department of Neurology, State Key Laboratory of Brain Function and Disorders, Ministry of Education Frontiers Center for Brain Science, Institutes of Brain Science, Zhongshan Hospital, Fudan University, Shanghai 200032, China

[2]Department of Rehabilitation Medicine, Zhongshan Hospital, Fudan University, Shanghai 200032, China

* Corresponding authors

* Zhuangzhi Zhang: zz_zhang@fudan.edu.cn

*Jing Ding: ding.jing@zs-hospital.sh.cn

*Xin Wang: wang.xin@zs-hospital.sh.cn

Graphical abstract

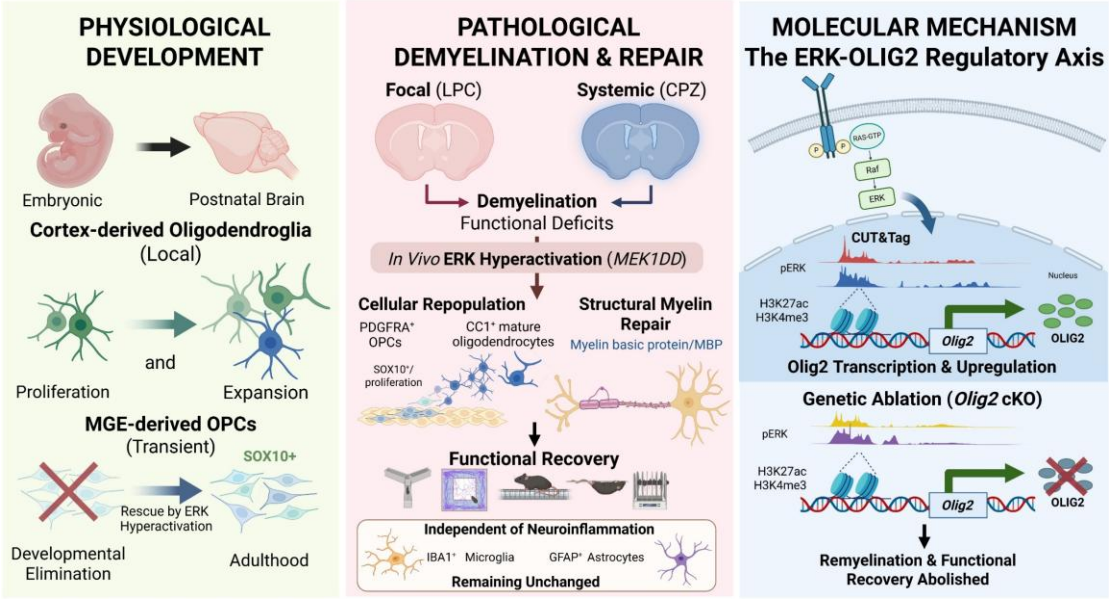

Highlights

- **Sustained ERK signaling rescues MGE-derived OPCs from developmental elimination.**
- **Targeted ERK hyperactivation drives in vivo myelin repair and functional recovery.**
- **ERK-promoted remyelination operates independently of neuroinflammation suppression.**
- **ERK directly targets *Olig2*, a transcription factor essential for myelin repair.**

ABSTRACT

The failure of myelin regeneration in demyelinating diseases, such as multiple sclerosis, is primarily driven by the depletion and maturation failure of oligodendrocyte precursor cells (OPCs). Here, we demonstrate that hyperactivation of extracellular signal-regulated kinase (ERK) signaling drives oligodendrocyte lineage expansion and structural myelin repair. During physiological development, sustained ERK activation promotes the proliferation, maturation, and survival of cortex-derived oligodendroglia and rescues medial ganglionic eminence (MGE)-derived OPCs from competitive elimination. In pathological contexts, using both lysolecithin (LPC)-induced focal demyelination and cuprizone (CPZ)-induced general demyelination models, targeted ERK hyperactivation drives the cellular repopulation of OPCs and restores demyelinated lesions. This structural repair directly ameliorates demyelination-induced motor and cognitive deficits. Furthermore, we show that the remyelination-promoting effects of ERK occur independently of a generalized suppression of neuroinflammation. Mechanistically, CUT&Tag-seq and *in vivo* rapid induction assays identify *Olig2* as a direct downstream transcriptional target of ERK. Conditional deletion of *Olig2* confirms that it is functionally indispensable for ERK-mediated myelin repair and behavioral recovery. Together, our findings elucidate a direct ERK-*Olig2* regulatory axis that governs oligodendrocyte lineage progression, providing a targeted and inflammation-independent therapeutic strategy for demyelinating disorders.

Keywords: multiple sclerosis; remyelination; oligodendrocyte precursor cells; MAPK/ERK signaling; *Olig2*

INTRODUCTION

Central nervous system (CNS) demyelinating diseases, such as multiple sclerosis (MS), are characterized by the progressive loss of myelin sheaths, leading to impaired axonal conduction and neurological dysfunction [1-3]. While spontaneous myelin repair (remyelination) can occur during the early stages of the disease, this capacity typically declines over time [4,5]. The failure of remyelination is primarily attributed to a hostile pathological microenvironment that prevents oligodendrocyte precursor cells (OPCs) from surviving, proliferating, and differentiating into mature oligodendrocytes at the lesion sites [6-8]. Consequently, identifying intrinsic molecular pathways that can expand the OPC pool and promote their maturation is a critical strategy for structural myelin repair and preventing long-term neurodegeneration [9,10].

Current approved therapeutics for MS predominantly rely on immunomodulatory agents designed to suppress neuroinflammation and reduce relapse rates [11]. However, these treatments exhibit limited efficacy in promoting direct myelin repair[12]. Furthermore, the complex interplay between neuroinflammation and myelin regeneration suggests that broadly suppressing the immune response may inadvertently alter beneficial glial functions required for tissue repair[13-15]. Therefore, it is critical to identify therapeutic targets that directly enhance the intrinsic regenerative capacity of the oligodendrocyte lineage, independent of systemic immunosuppression [16].

Extracellular signal-regulated kinase (ERK) signaling is a central intracellular pathway that integrates extracellular mitogenic signals to regulate cellular proliferation, survival, and differentiation[17-20]. Previous studies have implicated ERK signaling in the physiological development of the CNS and myelin growth[21-23]. However, the extent to which ERK can alter intrinsic, lineage-specific elimination programs during development, and its therapeutic potential across diverse pathological demyelinating environments, require further elucidation. More importantly, while ERK is fundamentally a cytoplasmic kinase cascade, its direct downstream transcriptional targets that mediate oligodendrocyte lineage progression and myelin repair *in vivo* remain largely unclear.

In this study, we demonstrate that sustained ERK activation not only promotes the expansion of cortex-derived oligodendroglia but also rescues medial ganglionic eminence (MGE)-derived OPCs from postnatal competitive elimination. Translating these developmental findings into pathological contexts, we show that targeted ERK hyperactivation drives cellular repopulation and myelin repair in both lysolecithin (LPC)-induced focal and cuprizone (CPZ)-induced general demyelination models. This repair significantly ameliorates demyelination-induced motor and cognitive deficits and occurs independently of generalized neuroinflammation suppression. Mechanistically, we re-analysis of published CUT&Tag-seq data and conditional knockout approaches, we identify *Olig2* as a direct downstream transcriptional target functionally required for ERK-mediated remyelination. Our findings establish the ERK-*Olig2* regulatory axis as a targeted, inflammation-independent therapeutic strategy for demyelinating disorders.

RESULTS

Enhanced ERK signaling drives the proliferation, maturation, and survival of locally generated cortical oligodendroglia

To investigate the *in vivo* function of ERK signaling in oligodendrocyte lineage cells, we employed a genetic strategy using the *IS* and *MEK1DD* mouse lines to conditionally hyperactivate ERK signaling (Figure 1A). To evaluate the impact of enhanced ERK signaling on cortex-derived oligodendroglia, we utilized *in utero* electroporation (IUE) to introduce Cre-expressing plasmids into the cortical radial glia of $IS^{F/+}$ and $IS^{F/+}$; *MEK1DD* embryos (Figure 1B). This approach allowed for the specific genetic manipulation of these progenitors while stably labeling them and their progeny with tdTomato (tdT, red).

Immunofluorescence analysis revealed a robust expansion of the oligodendrocyte lineage cell pool. Specifically, the number of $tdT^+/SOX10^+$ double-positive cells in both the cortex (Figure 1C, D) and the corpus callosum (Figure 1G, H) was significantly increased in the ERK-overexpressing group (hereafter referred to as *MEK1DD*) compared to the $IS^{F/+}$ group (hereafter referred to as Control) at postnatal day 30 (P30). Remarkably, this profound expansion was sustained into late adulthood, with $tdT^+/SOX10^+$ cell numbers remaining persistently elevated at P400 (Figure 1E-F and I-J). Consistent with the cellular expansion, enhanced ERK signaling also promoted oligodendrocyte maturation and cortical myelination. This was evidenced by a significant increase in myelin basic protein (MBP) fluorescent intensity and elevated *Mbp* mRNA density in the *MEK1DD* cortices at P400 (Figure S1A–D).

Enhanced ERK signaling rescues MGE-derived oligodendrocyte lineage cells from competitive elimination

Embryonic cortical OPCs originate from both the medial ganglionic eminence (MGE) and cortex-derived neural progenitors[24]; however, MGE-derived OPCs are known to be competitively eliminated and replaced by cortex-derived OPCs during adulthood[16] (Figure 2A). Building upon our observation that ERK signaling drives the expansion of locally generated OPCs, we hypothesized that ERK hyperactivation might alter the fate of these MGE-derived populations. By utilizing *Nkx2.1-Cre* mice to specifically enhance ERK signaling in MGE-derived progenitors (Figure 2B), we tracked the long-term survival of this distinct subpopulation. Strikingly, in contrast to the typical elimination observed in control cortices, the *Nkx2.1-Cre*; *MEK1DD* experimental group exhibited a significant increase in the number of $tdT^+/SOX10^+$ MGE-derived OPCs/OLs in both the motor and sensory cortices (Figure 2C, D), as well as the corpus callosum (Figure 2E, F), at both P30 and P60. Collectively, these developmental data demonstrate that sustained ERK activation fundamentally promotes the proliferation, maturation, and long-term survival of oligodendrocyte lineage cells, irrespective of their developmental origins (Figure 2G).

ERK hyperactivation promotes myelin repair and functional recovery following focal demyelination

To investigate the role of ERK signaling in pathological demyelination, we employed a focal demyelination model by stereotaxically injecting lysolecithin (LPC) into the corpus callosum of adult mice (Figure 3A). At 14 days post-injection (dpi), Luxol Fast Blue (LFB) and myelin basic protein (MBP) staining showed a significantly reduced demyelinated area in the corpus callosum of the *MEK1DD* group compared with the LPC control group (Figure 3B, C). This reduction in demyelination was maintained at 21 dpi (Figure S2A, B).

We next evaluated the behavioral outcomes associated with the histological changes. Motor function assessments revealed that the *MEK1DD* group exhibited an increased latency to fall in the rotarod test (Figure 3D), as well as reduced traverse time and paw slips in the beam walking test (Figure 3E). For cognitive evaluations, the *MEK1DD* mice showed restored spontaneous alteration in the Y-maze test (Figure 3F) and improved discrimination performance in the novel object recognition test (NORT) (Figure 3G).

To determine the cellular basis of this myelin repair, we analyzed the oligodendrocyte lineage cell population at the lesion site. Immunofluorescence analysis at 14 dpi showed that the *MEK1DD* group had an increased number of $PDGFRA^+$ oligodendrocyte precursor cells (OPCs) (Figure 4C), $CC1^+$ mature oligodendrocytes (Figure 4B), and $SOX10^+$ total lineage cells (Figure 4A) compared with the LPC control group. These cellular increases were also observed at the 21 dpi timepoint (Figure 4D–F). These results indicate that ERK hyperactivation facilitates myelin repair and functional recovery by promoting the expansion and maturation of OPCs following focal demyelination.

ERK hyperactivation promotes myelin repair and cellular repopulation in the cuprizone-induced general demyelination model

To determine whether the myelin repair effect of ERK signaling is applicable to a general demyelination context, we utilized the cuprizone (CPZ) dietary model. Histological analysis using Luxol Fast Blue (LFB) staining showed that the *MEK1DD* group exhibited an increased myelinated area in both the middle and lateral corpus callosum compared with the CPZ control group (Figure 5A-B). Consistent with the LFB staining, the *MEK1DD* group showed increased myelin basic protein (MBP) immunofluorescence intensity (Figure 5C-D) and elevated *Mbp* mRNA levels as detected by in situ hybridization (Figure 5E-F).

We next evaluated the behavioral outcomes. The open field test (OFT) revealed comparable baseline locomotion and anxiety-like behaviors across all groups, as indicated by total distance, center distance, frequency of center entries, and cumulative duration in the center zone (Figure 5G). In motor function assessments, the *MEK1DD* mice exhibited an increased latency to fall in the rotarod test (Figure

5H) and reduced traverse time and paw slips in the beam walking test (Figure 5I). For cognitive evaluations, the *MEK1DD* group showed restored spontaneous alteration in the Y-maze test (Figure 5J).

To investigate the cellular basis of this general myelin repair, we analyzed the oligodendrocyte lineage cell populations in the corpus callosum. Immunofluorescence analysis showed that the *MEK1DD* group had an increased number of PDGFRA$^+$ oligodendrocyte precursor cells (OPCs) (Figure 6A-B), CC1$^+$ mature oligodendrocytes (Figure 6C-D), and SOX10$^+$ total lineage cells (Figure 6E-F) compared with the CPZ control group. Furthermore, the number of SOX10$^+$/KI67$^+$ proliferating oligodendrocyte lineage cells was increased in the *MEK1DD* group (Figure 6E-F), indicating that the restoration of the SOX10$^+$ cell pool was driven by increased cellular proliferation. These results indicate that ERK hyperactivation promotes myelin repair and functional recovery in a general demyelination model by driving the proliferation and expansion of oligodendrocyte lineage cells.

The remyelination-promoting effects of ERK are independent of global neuroinflammation

To determine whether the enhanced myelin repair in the *MEK1DD* mice was influenced by changes in the neuroinflammatory environment, we assessed microglial and astrocytic activation in both the focal and general demyelination models. In the LPC-induced focal demyelination model, immunofluorescence analysis of IBA1 (a microglial marker) and GFAP (an astrocytic marker) revealed increased numbers of IBA1$^+$ and GFAP$^+$ cells at the lesion site compared with the sham group. However, there was no significant difference in the number of IBA1$^+$ or GFAP$^+$ cells between the *MEK1DD* and LPC control groups at either 14 dpi (Figure S3A–D) or 21 dpi (Figure S3E–H). Similarly, in the CPZ-induced general demyelination model, both the *MEK1DD* and CPZ control groups exhibited comparable increases in IBA1$^+$ (Figure S3I-J) and GFAP$^+$ (Figure S3K-L) cell numbers relative to the healthy controls. These results indicate that the remyelination-promoting effects of ERK hyperactivation occur independently of a generalized modulation of neuroinflammation, suggesting a direct role within the oligodendrocyte lineage.

ERK directly targets *Olig2* to mediate oligodendrocyte lineage progression and myelin repair

To investigate the downstream molecular mechanisms underlying ERK-mediated oligodendrocyte lineage expansion, we re-analysis of published CUT&Tag-seq data[25] (Figure 7A). Genomic analysis identified binding peaks of phosphorylated ERK (pERK) at the regulatory regions of the *Olig1* and *Olig2* loci, which co-localized with the active chromatin marks H3K27ac and H3K4me3 (Figure 7B).

To validate whether *Olig2* is a direct downstream target of ERK *in vivo*, we utilized *in utero* electroporation (IUE) targeting the embryonic cortex at E15.5. Immunofluorescence analysis at E16.5, just 24 hours post-electroporation, showed that ERK hyperactivation (*MEK1DD*) induced an upregulation of OLIG2 expression in the electroporated cells compared with the control (Figure 7C). This rapid induction supports *Olig2* as a direct downstream target of ERK signaling.

Next, we investigated whether OLIG2 is functionally required for the ERK-mediated remyelination. We introduced a conditional *Olig2* knockout into the *MEK1DD* background (*Olig2*$^{F/F}$; *MEK1DD*) and evaluated myelin repair in the focal LPC demyelination model. Histological analysis using MBP staining showed that the reduction in demyelinated area observed in the *MEK1DD* group was abolished by the concurrent deletion of *Olig2* (Figure 7D-E). Consistent with the histological findings, behavioral assessments demonstrated that the improvements in motor and cognitive performance achieved by *MEK1DD*, as measured by the rotarod test (Figure 7F), beam walking test (Figure 7G), and Y-maze test (Figure 7H), were reversed in the *Olig2*$^{F/F}$; *MEK1DD* group. These results indicate that OLIG2 is functionally indispensable for the myelin repair and functional recovery driven by ERK hyperactivation.

DISCUSSION

The failure of remyelination in demyelinating diseases such as multiple sclerosis (MS) is primarily attributed to the inability of oligodendrocyte precursor cells (OPCs) to survive, proliferate, and differentiate at lesion sites [7,26]. In this study, we demonstrate that conditionally hyperactivating ERK signaling (*MEK1DD*) overcomes these barriers. We establish that ERK signaling is not only fundamental for the physiological expansion of cortical oligodendroglia but also serves as a potent driver for myelin repair and functional recovery in pathological demyelination.

During cortical development, OPCs originate from both the medial ganglionic eminence (MGE) and local cortical progenitors, yet the MGE-derived population is competitively eliminated during postnatal maturation[16,24,27]. Our developmental data reveal that sustained ERK activation rescues these MGE-derived OPCs from developmental elimination, allowing them to persist into adulthood. This finding indicates that ERK signaling operates as a dominant survival and proliferation signal that can override intrinsic, lineage-specific elimination programs. By demonstrating this fundamental biological principle, we provided the rationale for manipulating ERK to restore the depleted OPC pool in demyelinating diseases.

Translating this developmental mechanism to pathological contexts, we investigated the therapeutic potential of the ERK pathway using two distinct demyelination models: LPC-induced focal demyelination and CPZ-induced general demyelination. In both models, ERK hyperactivation driven by *MEK1DD* promoted the cellular repopulation of PDGFRA$^+$ OPCs and CC1$^+$ mature oligodendrocytes, which

subsequently translated into histological myelin repair and the restoration of motor and cognitive functions. The consistent protective effects across the focal (LPC) and general (CPZ) paradigms suggest that targeting ERK signaling provides a broad-spectrum strategy for demyelinating conditions, independent of the initial demyelinating insult [20,21].

A major challenge in current MS therapies is the complex interplay between neuroinflammation and myelin repair [6,28]. While current immunomodulatory drugs reduce relapse rates, they generally fail to promote remyelination[11]. Previous studies have established that modulating the neuroinflammatory environment—such as promoting the polarization of microglia toward an anti-inflammatory phenotype or pharmacologically suppressing neuroinflammation—can significantly enhance CNS remyelination [13,14]. However, our evaluation of the neuroinflammatory environment revealed that the remyelination-promoting effects of ERK hyperactivation occurred without significantly altering the generalized activation of microglia ($IBA1^+$) or astrocytes ($GFAP^+$) at the demyelinated lesions. The comparable levels of reactive gliosis between the *MEK1DD* and control groups across models indicate that ERK facilitates myelin repair through intrinsic mechanisms within the oligodendrocyte lineage, rather than secondary to a broad suppression of neuroinflammation. This uncoupling of remyelination from general immunosuppression highlights the ERK pathway as a direct, lineage-specific target for regenerative therapies.

Mechanistically, we identified *Olig2* as a direct downstream target of ERK in regulating oligodendrocyte lineage progression. While ERK is a known kinase primarily associated with cytoplasmic signaling cascades, our CUT&Tag analysis revealed the accumulation of phosphorylated ERK at the regulatory regions of the *Olig2* locus, co-localized with active transcription marks. The rapid induction of OLIG2 following *in utero* electroporation further confirmed this direct regulatory axis. More importantly, the genetic deletion of *Olig2* in the *MEK1DD* background completely abolished the remyelination and functional recovery observed in the LPC model. *Olig2* is a master transcription factor essential for oligodendrocyte specification and differentiation[25,29,30]. Our data bridge the gap between extracellular mitogenic signals and core transcriptional programs, demonstrating that ERK mediates structural myelin repair by directly sustaining *Olig2* expression.

In conclusion, our study identifies the ERK-*Olig2* signaling axis as a critical regulator of oligodendrocyte lineage expansion and myelin repair. By promoting the proliferation, maturation, and survival of OPCs independently of the neuroinflammatory environment, manipulating ERK signaling offers a targeted therapeutic approach to promote remyelination and restore neurological function in demyelinating disorders.

MATERIALS AND METHODS

Animals

The transgenic mouse lines used in this study included the *IS*[31] (Cre-dependent reporter), *MEK1DD* [18] (Cre-dependent conditionally hyperactivated ERK signaling), *Nkx2.1-Cre* [32], and *Olig2*$^{F/F}$ [25] (conditional knockout) mice. Mice were housed in a specific pathogen-free facility under a standard 12 h light/12 h dark cycle with ad libitum access to food and water. For embryo collection and *in utero* electroporation (IUE), the morning a vaginal plug was observed was designated as embryonic day 0.5 (E0.5), and the day of birth as postnatal day 0 (P0).

Euthanasia and tissue preparation

All animal procedures and euthanasia protocols were approved by the Animal Ethics Committee of Fudan University Shanghai Medical College (Approval No. 20220228-140) and conducted in accordance with institutional guidelines and the American Veterinary Medical Association (AVMA) Guidelines for the Euthanasia of Animals. For histological analysis, mice were deeply anesthetized via an intraperitoneal injection of sodium pentobarbital (100 mg/kg). Unconsciousness and a deep surgical plane of anesthesia were confirmed by the complete absence of the pedal withdrawal (toe-pinch) reflex. Mice were then euthanized by exsanguination via transcardial perfusion with phosphate-buffered saline (PBS), followed by 4% paraformaldehyde (PFA) in PBS. This method was chosen to minimize animal pain and distress while ensuring rapid blood clearance and optimal preservation of brain and myelin structure for histological analysis. All brains were post-fixed overnight in 4% PFA at 4℃, followed by cryoprotection in 30% sucrose for at least 24 hours. Tissue samples were embedded in Optimal Cutting Temperature (O.C.T.) compound (Sakura Finetek), flash-frozen in a dry ice/ethanol slurry, and stored at -80℃ until sectioning.

In utero electroporation (IUE)

In utero electroporation (IUE) of embryos was performed at E15.5. The *pCAG-Cre* plasmid was mixed with 0.05% Fast Green (Sigma) and injected into the lateral ventricle of embryos (0.5 μl per embryo) using a beveled glass micropipette. Five electrical pulses (duration: 50 ms) were applied across the uterus to E15.5 embryos at 35 V. The interval between pulses is 950ms. Electroporation was performed using a pair of 7 mm platinum electrodes (BTX, Tweezerrode 45-0488, Harvard Apparatus) connected to an electrocleaner (BTX, ECM830). Uterine horns were repositioned into the abdominal cavity before the abdominal wall and the skin were sutured.

CUT&Tag data re-analysis

There was no *de novo* high-throughput sequencing performed in this study. The CUT&Tag-seq datasets utilized for analyzing the binding peaks of phosphorylated ERK (pERK) and active chromatin marks (H3K27ac and H3K4me3) at the *Olig1* and *Olig2* loci were obtained from previously published datasets. Originally, these data were generated using FACS-sorted GFP^{+} cells isolated from the cortices of *hGFAP-*

GFP mice at E18.5-P1. The raw datasets were re-aligned and visualized using standard genomic browser tools to identify direct transcriptional targets of ERK signaling in the context of oligodendrocyte lineage progression.

Immunofluorescence

The tissue sections were first washed with 0.05 M TBS for 10 minutes, then incubated in Triton-X-100 (0.5% in 0.05 M TBS) for 30 minutes at room temperature (RT). Following this, the sections were incubated with blocking solution (5% donkey serum + 0.5% Triton-X-100 in 0.05 M TBS, pH 7.2) for 2 hours at RT. Primary antibodies, diluted in 5% donkey serum, were applied and incubated overnight at 4℃. Afterward, the sections were rinsed three times with 0.05 M TBS. Secondary antibodies (1:500, all from Jackson ImmunoResearch) specific to the appropriate species were added and incubated for 2 hours at RT. Fluorescently stained sections were then washed three times with 0.05 M TBS for 10 minutes each. The sections were subsequently stained with 4',6-diamidino-2-phenylindole (DAPI) (1:3000, Sigma) diluted in TBS for 1 minute and rinsed three more times with TBS. Finally, the sections were coverslipped with Gel/Mount (Biomeda, Foster City, CA).

The following primary antibodies were used in this study: goat anti tdT (tdTomato, 1:2000, SICGEN, Ab8181), goat anti-SOX10 (1:500, R&D System, AB-442208), guinea pig anti-SOX10 (1:500, Oasis Biofarm, OB-PGP001), rabbit anti-PDGFRA (1:500, Oasis Biofarm, OB-PRB051), rabbit anti-MBP (1:500, Oasis Biofarm, OB-PRB130), rat anti-CC1 (1:1000, Oasis Biofarm, OB-PRT039), rabbit anti-I67(1:2000, Abcam, ab15580), guinea pig anti-IBA1 (1:500, Oasis Biofarm, OB-PGP049), rat anti-GFAP (1:1000, Invitrogen, Cat# 13-0300), chicken anti-GFP (1:3000, Aves labs, GFP-1020), rabbit anti-OLIG2 (1:500, Millipore, AB9610), rat anti-OLIG2 (1:500, Oasis Biofarm, OB-PRB009-01).

***In situ* hybridization**

In situ hybridization (ISH) was performed as previously described [33]. Briefly, ISH was performed on 16μm cryosections using digoxigenin riboprobes. Probes were made from P0 wild-type mouse brain cDNA amplified by PCR using the following primers:
Primer F (Mbp): cgcggatccgaagagacagccgctctggatctc; and
Primer R (Mbp): ccggaattcatggtgacatttggcggccac.

Luxol fast blue staining

Luxol fast blue (LFB) staining was used for histological assessment of damage in the white matter. Briefly, 16μm brain sections were incubated in preheated 0.1% LFB dye (Servicebio, G1030) at 60℃ for 6-8 hours. The sections were cooled to room temperature and rinsed gently under running water for 5 min, followed by differentiated in 0.05% Li_2CO_3 solution and terminated in 75% ethanol. And then sections were sequentially dehydrated through 75%-90%-100% ethanol. Images of

staining were taken by an Olympus optical microscope. The area of demyelination in corpus callosum was calculated using ImageJ.

LPC-induced demyelination model

Focal demyelination models were induced by two-point lysophosphatidylcholine (LPC) injection procedure as described [34]. Briefly, adult (8–12 weeks) mice were deeply anesthetized with isoflurane (induced at 3%, and maintained at 1.5%), positioned into a stereotaxic frame (RWD Life Science, China). The first injection site was 1.0 mm lateral to the bregma, 0.6 mm anterior to the bregma, and 2.1 mm ventral to the skull. The second injection site was 1.0 mm lateral to the bregma, 1.1 mm anterior, and 2.4 mm deep. Each site was injected with 2 μl of 1% LPC (Sigma, USA, Cat#L4129) in sterile saline solution at a rate of 0.5 μl/min. Mice in sham group were injected with 2 μl saline at each point. Ten minutes after the delivery of LPC solution, the needle was slowly retracted. After injection, mice were sacrificed at 14 dpi and 21 dpi in each group, separately. Adeno-associated virus (AAV)-PHP.eB-CAG-EGFP-P2A-Cre-WPRE were produced by OBiO Technology Inc. (Shanghai, China). 0.2 μl AAV-Cre (1×10^{12} vg/ml) was injected into the same site 7 days before to LPC injection.

CPZ-induced demyelination model

Male mice were fed with 0.3% cuprizone (CPZ, Sigma, C9012) pellets for a duration of 45 days. Control mice were fed normal chow. During the experiment, all animals had access to chow and water without restrictions. Experiments were conducted in animals at 8-12 weeks of age. Following 1–2 weeks of CPZ diet feeding, AAV-Cre (1×10^{12} vg/ml) was stereotaxically delivered into the bilateral lateral ventricles at 2 μl per side. The injection site was 1.0 mm lateral to the bregma, 0.5 mm posterior, and 1.8 mm deep. Functional behavioral tests were performed after 5-6 weeks of CPZ diet feeding, and mice were sacrificed on day 45 for tissue collection.

Open field test

Open field test (OFT) can be used to analyze autonomous activity and explore the behaviors of rodents under novel circumstances. The apparatus was a 40 cm × 40 cm square area with 30 cm-high sidewalls. Mice were allowed to move freely in the apparatus and probe the space for 10 min. The video camera was placed above the square to record their movement. Data were obtained by Noldus EthoVision XT system, an automatic animal behavior recording system, such as total distance, center distance, etc.

Novel object recognition test

Novel object recognition (NOR) test has been widely used to detect memory function. The apparatus was a 40 cm × 40 cm square area with 30 cm-high sidewalls. During the familiar stage, two identical objects were placed in the box, and mice were allowed to explore freely in 6 min. The test trial was conducted after 30 min. The

mice were returned to the apparatus in which one of the original objects was replaced by a novel object of similar size (“novel”), while the other object remained unchanged (“familiar”). During the test phase, the exploration time for mice was 6 min, and the apparatus was cleaned with 75% ethanol to avoid any interference with subsequent tests between each trial. The video recordings were analyzed using the Noldus EthoVision XT system. Discrimination index (DI) = (N − F)/(N + F) × 100% (N = time spent exploring the “novel” object and F = time spent exploring the “familiar” object). Discrimination Ratio = N / (N + F) × 100%.

Y-maze

We used the Y-maze apparatus to measure the working memory by noting spontaneous alternation. Mice are naturally inclined to explore new environments. Normal mice can memorize the arm they have explored and enter the other arm of the maze. Mice were allowed to stay at the end of one arm and explore all the other arms for 8 min. We named three arms A, B, and C, respectively. Alternations defined as overlapping entry sequences (such as ABC, BCA) were counted as a percentage: spontaneous alternation = (alternation times)/(total number of arm entries − 2) × 100%.

Rotarod test

To evaluate limb motor coordination and balance of mice, the rotarod test was performed. Before testing, mice underwent 3 days of adaptation training in the rotarod apparatus. On the test day, the latency of falling off the rotarod (Ugo Basile, Italy) with a linear increase in rod speed from 4 rpm up to 40 rpm in 5 min was measured three times. Each mouse was tested 3 times for repeated testing the latency to fall and calculated the average as results.

Beam walking test

The beam walking test was performed to assess the coordination and balance of mice. A balance beam (1 m × 1 cm) was placed 50 cm above the floor, with a bedding-filled safety box positioned at its end. Start and end lines were marked on the beam and were 80 cm apart. The mice were trained to enter the safety box through the balance beam one day before testing. On the test day, each mouse underwent two trials, with at least 10 min between trials. The average traverse time and the times of paws slip by each mouse were recorded.

Image acquisition

Whole-slide imaging was performed using an Olympus VS120 slide scanner with 10X or 20X objectives. High-resolution fluorescence imaging was conducted on an Olympus FV3000 confocal microscope system equipped with 10X, 20X, and 40X objectives. All images were processed (merged, cropped, and contrast-adjusted) using Adobe Photoshop and Illustrator software while maintaining data integrity.

Quantification and statistical analysis

In this study, all cell counts were performed on the imaged sections collected by Olympus VS120 Automated Slide Scanner with 10X. At least three samples of control or mutant mice were examined. The analyzed mice were littermates of both sexes and ages matched. Investigators were not blinded to mouse genotypes during analysis. Values and error bars represent the mean ± SEM. The respective replicate number (n) is indicated in the figures. All the measurements were done using sections that match the same anterior–posterior level. At least three matching sections from each brain were used for measurement and compared between mutant and control littermates. Statistical comparisons were performed using P-values determined by an appropriate statistical test, such as the Student's t-test for two groups with normally distributed data. For most analyses, one-way analysis of variance (ANOVA) was followed by Tukey's test for multiple comparisons. Analyses were performed using GraphPad Prism 8.0. ImageJ software was applied to evaluate the expression level, which was determined by integrated fluorescence density. A value of $P < 0.05$ was considered to indicate statistical significance.

DECLARATIONS

Abbreviations

ERK: Extracellular signal-regulated kinase

Olig2：Oligodendrocyte transcription factor 2

OPC: Oligodendrocyte precursor cells

MGE: Medial ganglionic eminence

LPC: lysolecithin

CPZ: Cuprizone

CNS: Central nervous system

MS: Multiple sclerosis

IUE: *In utero* electroporation

TdT: TdTomato

MBP: Myelin basic protein

LFB: Luxol Fast Blue

NORT: Novel object recognition test

PDGFRA: Platelet derived growth factor receptor alpha

SOX10: SRY-box transcription factor 10

OFT: open field test

IBA1: Ionized calcium-binding adapter molecule 1

GFAP: Glial fibrillary acidic protein

CUT&Tag-seq: Cleavage under targets and tagmentation

PBS: Phosphate-buffered saline

ISH: In situ hybridization

ANOVA: One-way analysis of variance test

Ethics approval and consent to participate

All animal procedures were approved by the Animal Ethics Committee of Fudan University Shanghai Medical College and conducted in accordance with institutional guidelines (Approval No. 20220228-140).

Consent for publication

Not applicable.

Availability of data and materials

The previously published CUT&Tag-seq data analyzed in this study are available in the NCBI GEO repository under accession number GSE275004. All other data that support the findings of this study are available from the corresponding author upon reasonable request.

Competing Interests

The authors declare no conflict of interest.

Funding

This study was supported by the National Natural Science Foundation of China (Grant NO.82271499 and 32200776).

Authors' contributions

J.L., F.Y., W.Z., D.H., Z.S., D.Q. performed the experiments. J.L., F.Y., designed the experiments, produced figures, and edited the manuscript with input from all authors. Z.Z., D.J, and X.W. conceptualized, supervised the project, and wrote the manuscript. All authors contributed to the article and approved the submitted version.

Acknowledgments

Not applicable.

Reference:

1 Reich, D. S., Lucchinetti, C. F. & Calabresi, P. A. Multiple Sclerosis. *The New England journal of medicine* **378**, 169-180, doi:10.1056/NEJMra1401483 (2018).

2 Compston, A. & Coles, A. Multiple sclerosis. *Lancet (London, England)* **372**, 1502-1517, doi:10.1016/s0140-6736(08)61620-7 (2008).

3 Al-Otaibi, K. M. Evaluation of the Behavioral and Histopathological Outcomes of Two Cuprizone Administration Routes in a Mouse Model of Multiple Sclerosis. *J Integr Neurosci* **25**, 52589, doi:10.31083/JIN52589 (2026).

4 Franklin, R. J. M. & ffrench-Constant, C. Regenerating CNS myelin — from mechanisms to experimental medicines. *Nature Reviews Neuroscience* **18**, 753-769, doi:10.1038/nrn.2017.136 (2017).

5 Lubetzki, C., Zalc, B., Williams, A., Stadelmann, C. & Stankoff, B. Remyelination in multiple sclerosis: from basic science to clinical translation. *The Lancet. Neurology* **19**, 678-688, doi:10.1016/S1474-4422(20)30140-X (2020).

6 Hess, K. *et al.* Lesion stage-dependent causes for impaired remyelination in MS. *Acta neuropathologica* **140**, 359-375, doi:10.1007/s00401-020-02189-9 (2020).

7 Liu, X. *et al.* Small-molecule-induced epigenetic rejuvenation promotes SREBP condensation and overcomes barriers to CNS myelin regeneration. *Cell* **187**, 2465-2484.e2422, doi:10.1016/j.cell.2024.04.005 (2024).

8 Wang, Y. *et al.* Microenvironmental Regulation of Central Nervous System Myelination and Remyelination. *J Integr Neurosci* **25**, 43257, doi:10.31083/JIN43257 (2026).

9 Li, N. *et al.* Vitamin D Promotes Remyelination by Suppressing c-Myc and Inducing Oligodendrocyte Precursor Cell Differentiation after Traumatic Spinal Cord Injury. *Int J Biol Sci* **18**, 5391-5404, doi:10.7150/ijbs.73673 (2022).

10 Gu, L. *et al.* Single-cell and Spatial Transcriptomics Reveals Ferroptosis as The Most Enriched Programmed Cell Death Process in Hemorrhage Stroke-induced Oligodendrocyte-mediated White Matter Injury. *Int J Biol Sci* **20**, 3842-3862, doi:10.7150/ijbs.96262 (2024).

11 Plemel, J. R., Liu, W.-Q. & Yong, V. W. Remyelination therapies: a new direction and challenge in multiple sclerosis. *Nature Reviews Drug Discovery* **16**, 617-634, doi:10.1038/nrd.2017.115 (2017).

12 Domingues, H. S., Portugal, C. C., Socodato, R. & Relvas, J. B. Oligodendrocyte, Astrocyte, and Microglia Crosstalk in Myelin Development, Damage, and Repair. *Front Cell Dev Biol* **4**, 71, doi:10.3389/fcell.2016.00071 (2016).

13 Miron, V. E. *et al.* M2 microglia and macrophages drive oligodendrocyte differentiation during CNS remyelination. *Nat Neurosci* **16**, 1211-1218, doi:10.1038/nn.3469 (2013).

14 Lloyd, A. F. & Miron, V. E. The pro-remyelination properties of microglia in the central nervous system. *Nat Rev Neurol* **15**, 447-458, doi:10.1038/s41582-019-0184-2 (2019).

15 Liddelow, S. A. & Barres, B. A. Reactive Astrocytes: Production, Function, and Therapeutic Potential. *Immunity* **46**, 957-967, doi:10.1016/j.immuni.2017.06.006 (2017).

16 Kessaris, N. *et al.* Competing waves of oligodendrocytes in the forebrain and postnatal elimination of an embryonic lineage. *Nat Neurosci* **9**, 173-179, doi:10.1038/nn1620 (2006).

17 Gao, Y. *et al.* NOTCH, ERK, and SHH signaling respectively control the fate determination

of cortical glia and olfactory bulb interneurons. *Proc Natl Acad Sci U S A* **122**, e2416757122, doi:10.1073/pnas.2416757122 (2025).

18 Zhang, Z. *et al.* Integrated ERK-PKA-YAP/TAZ-SHH Signaling Orchestrates Cortical Radial Glia Identity and Lineage Diversification. *Advanced science (Weinheim, Baden-Wurttemberg, Germany)* **13**, e13571, doi:10.1002/advs.202513571 (2026).

19 Li, J. *et al.* Molecular signatures and lineage diversification of neurogenic and gliogenic radial glia in the gyrencephalic ferret cortex. *Commun Biol*, doi:10.1038/s42003-026-10366-x (2026).

20 Jeffries, M. A. *et al.* ERK1/2 Activation in Preexisting Oligodendrocytes of Adult Mice Drives New Myelin Synthesis and Enhanced CNS Function. *J Neurosci* **36**, 9186-9200, doi:10.1523/JNEUROSCI.1444-16.2016 (2016).

21 Fyffe-Maricich, S. L., Schott, A., Karl, M., Krasno, J. & Miller, R. H. Signaling through ERK1/2 controls myelin thickness during myelin repair in the adult central nervous system. *J Neurosci* **33**, 18402-18408, doi:10.1523/JNEUROSCI.2381-13.2013 (2013).

22 Furusho, M., Kaga, Y., Ishii, A., Hebert, J. M. & Bansal, R. Fibroblast growth factor signaling is required for the generation of oligodendrocyte progenitors from the embryonic forebrain. *J Neurosci* **31**, 5055-5066, doi:10.1523/JNEUROSCI.4800-10.2011 (2011).

23 Liu, T. *et al.* The Role of SPTLC2 and the MEK/ERK Signaling Pathway in the Metabolic Activity and Proliferation of Neural Stem Cells. *J Integr Neurosci* **25**, 52923, doi:10.31083/JIN52923 (2026).

24 Li, J. *et al.* Lateral/caudal ganglionic eminence makes limited contribution to cortical oligodendrocytes. *eLife* **13**, doi:10.7554/eLife.94317 (2024).

25 Tian, Y. *et al.* Olig1/2 Orchestrates Progenitor Cell Fates during Mammalian Cortical Gliogenesis and Gliomagenesis. *Nat Commun* **16**, 9779, doi:10.1038/s41467-025-64753-9 (2025).

26 Duncan, G. J. *et al.* Myelin regulatory factor drives remyelination in multiple sclerosis. *Acta neuropathologica* **134**, 403-422, doi:10.1007/s00401-017-1741-7 (2017).

27 Richardson, W. D., Kessaris, N. & Pringle, N. Oligodendrocyte wars. *Nat Rev Neurosci* **7**, 11-18, doi:10.1038/nrn1826 (2006).

28 Mironova, Y. A. *et al.* Myelin is repaired by constitutive differentiation of oligodendrocyte progenitors. *Science* **391**, eadu2896, doi:10.1126/science.adu2896 (2026).

29 Wang, Z. *et al.* Coordinated regulation of cortical astrocyte maturation by OLIG1 and OLIG2 through BMP7 signaling modulation. *J Genet Genomics* **52**, 1224-1237, doi:10.1016/j.jgg.2025.03.008 (2025).

30 Yu, Y. *et al.* Olig2 Targets Chromatin Remodelers to Enhancers to Initiate Oligodendrocyte Differentiation. *Cell* **152**, 248-261, doi:10.1016/j.cell.2012.12.006 (2013).

31 Li, X. *et al.* Decoding Cortical Glial Cell Development. *Neurosci Bull* **37**, 440-460, doi:10.1007/s12264-021-00640-9 (2021).

32 Liu, Z. *et al.* Sp9 Regulates Medial Ganglionic Eminence-Derived Cortical Interneuron Development. *Cereb Cortex* **29**, 2653-2667, doi:10.1093/cercor/bhy133 (2019).

33 Li, Z. *et al.* Transcription factor Sp9 is a negative regulator of D1-type MSN development. *Cell Death Discovery* **8**, doi:10.1038/s41420-022-01088-0 (2022).

34 Luo, Q. *et al.* A stable and easily reproducible model of focal white matter demyelination. *J Neurosci Methods* **307**, 230-239, doi:10.1016/j.jneumeth.2018.05.024 (2018).

Figures

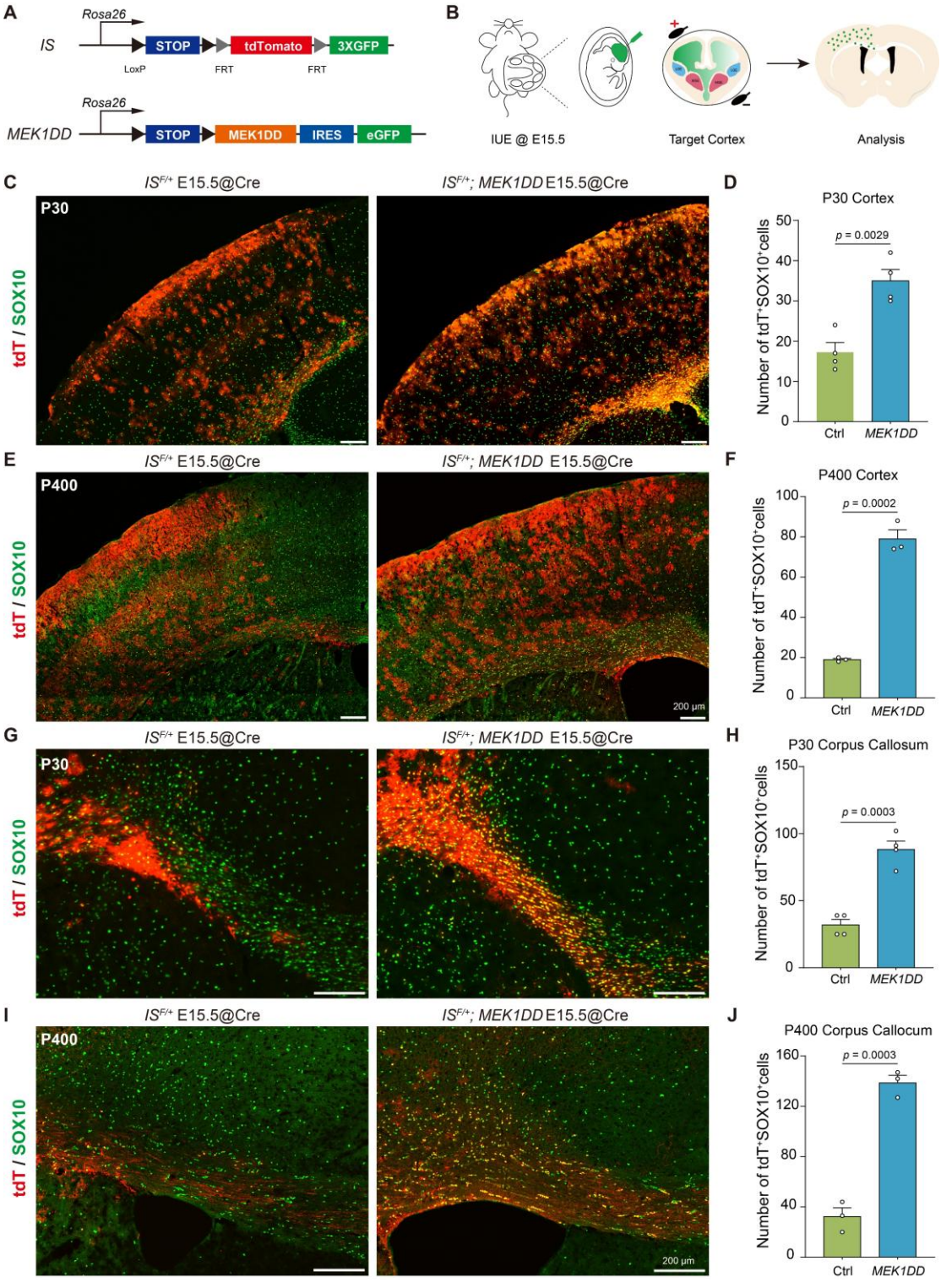

Figure 1: Enhanced ERK signaling drives the proliferation and survival of resident cortical oligodendroglia.

(**A**) Schematic representation of the genetic strategy used to generate the *IS* and *MEK1DD* mouse lines.

(**B**) Schematic diagram of *in utero* electroporation (IUE) utilized to investigate the *in vivo* function of ERK signaling in the mouse cortex.

(**C, D**) Representative immunohistochemistry images (C) and quantification (D) showing a significant increase in the number of tdT^+ /$SOX10^+$ double-positive cells in the cortex of the ERK-overexpressing group (*$IS^{F/+}$; MEK1DD*) compared to the control group (*$IS^{F/+}$*) at postnatal day 30 (P30).

(E, F) Representative images (E) and quantification (F) demonstrating a sustained increase in cortical tdT^+ /$SOX10^+$ double-positive cells in the ERK-overexpressing group versus the control group at P400.

(G, H) Representative images (G) and quantification (H) of the corpus callosum at P30, revealing a significantly higher number of tdT^+ /$SOX10^+$ cells in the ERK-overexpressing group relative to the control group.

(I, J) Representative images (I) and quantification (J) of the corpus callosum at P400, indicating a persistent elevation in tdT^+ /$SOX10^+$ cell numbers in the ERK-overexpressing group compared to the control group. ($n \geqslant 3$ per group; mean $\pm$ SEM; unpaired two-tailed Student's *t* test with Welch's correction).

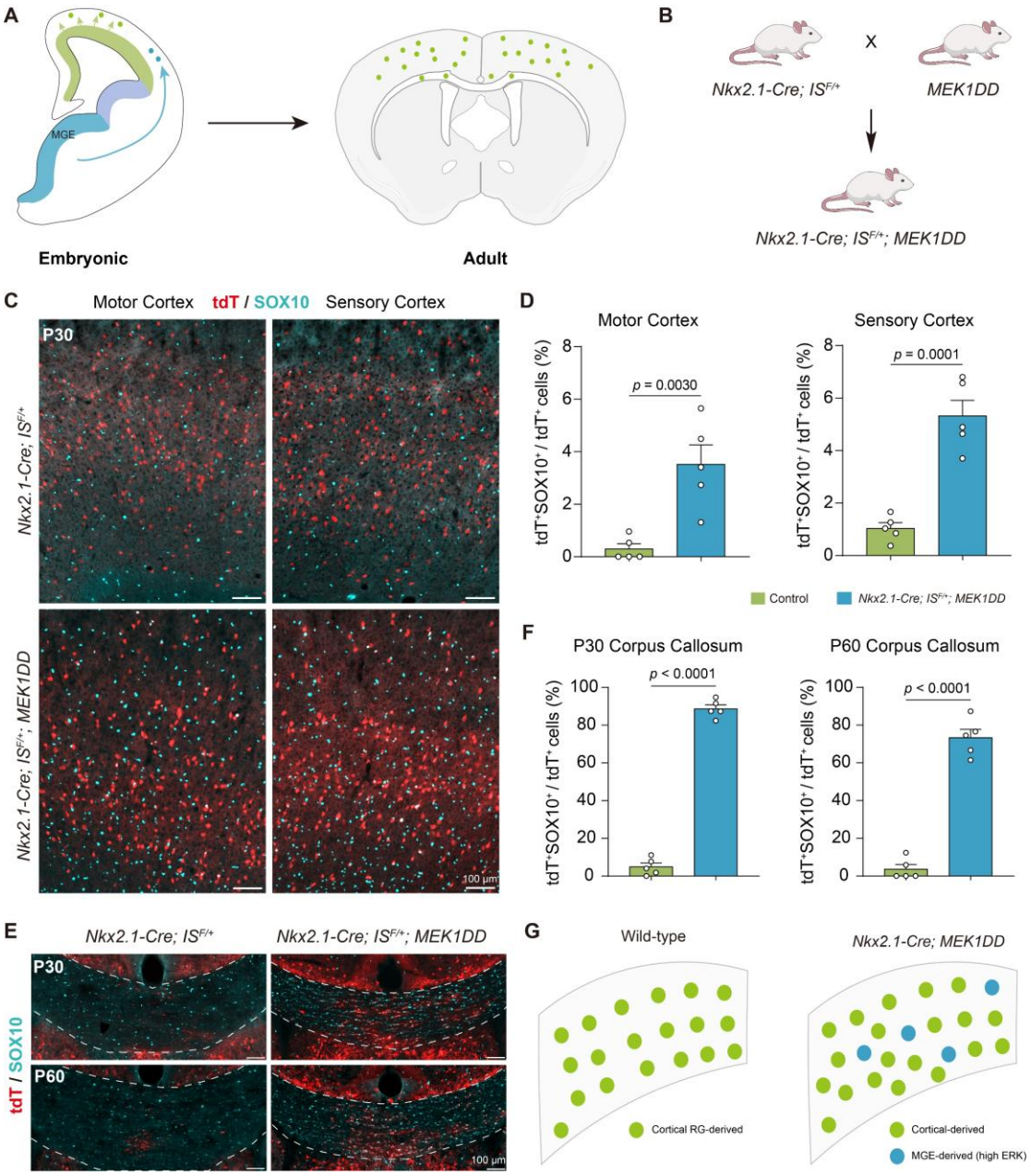

Figure 2: Enhanced ERK signaling rescues MGE-derived oligodendroglia from competitive elimination.

(A) Schematic model illustrating the developmental origins and ultimate survival of cortical OPCs. Embryonic cortical OPCs originate from both the medial ganglionic eminence (MGE) and cortical neural progenitors; however, MGE-derived OPCs are competitively replaced by cortex-derived OPCs during adulthood.

(B) Breeding strategy for generating mouse lines with specifically enhanced ERK signaling in MGE-derived OPCs using *Nkx2.1-Cre*.

(C, D) Representative immunohistochemistry images (C) and quantification (D) showing a significant increase in the number of tdT^+ /$SOX10^+$ double-positive cells in both the motor and sensory cortices of the *Nkx2.1-Cre; IS$^{F/+}$; MEK1DD* compared to

the control group (*Nkx2.1-Cre; IS$^{F/+}$*) at P30.

(E, F) Representative images (E) and quantification (F) of the corpus callosum at P30 and P60, demonstrating a significantly higher number of tdT^{+} /SOX10^{+} cells in the *Nkx2.1-Cre; IS$^{F/+}$; MEK1DD* relative to the control group.

(G) In wild-type adult mice, the cortex is populated exclusively by cortex-derived OPCs. Conversely, upon acquiring enhanced ERK signaling, MGE-derived OPCs survive into adulthood. This rescues MGE-derived cells from competitive elimination, further confirming the critical role of ERK in promoting OPC survival. (n = 5 per group; mean ± SEM; unpaired two-tailed Student's *t* test with Welch's correction).

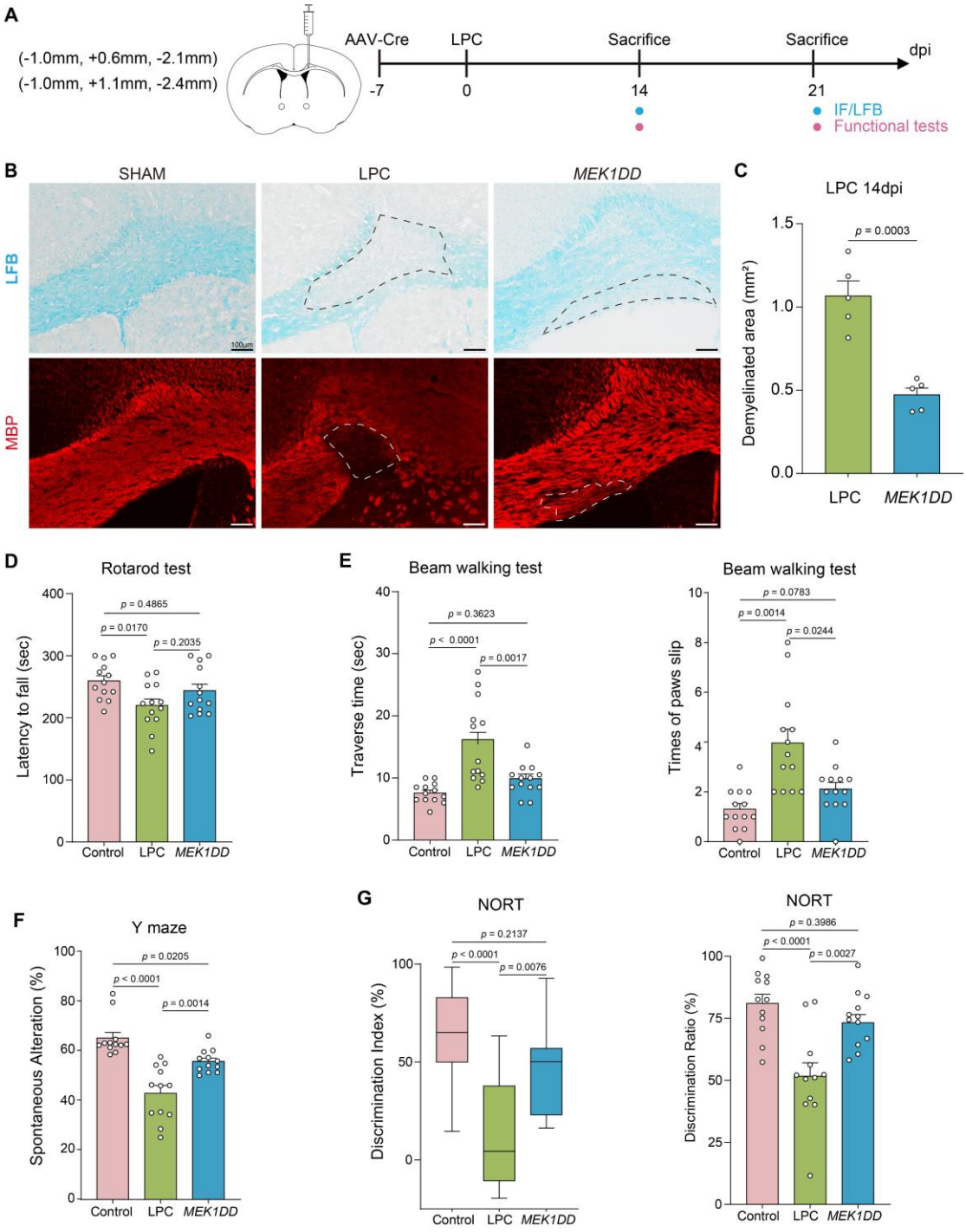

Figure 3. Enhanced ERK signaling protects against LPC-induced demyelination and associated neurobehavioral deficits.

(A) Schematic diagram of the experimental timeline for stereotaxic LPC injection and subsequent behavioral and histological analyses.

(B, C) Representative Luxol Fast Blue (LFB) and myelin basic protein (MBP) staining images (B) and quantification (C) demonstrating a significantly reduced demyelinated area in the corpus callosum of the ERK-overexpressing group (*MEK1DD*) compared

to the LPC control group at 14 days post-injection (dpi). (n = 5 per group; mean ± SEM; unpaired two-tailed Student's *t* test with Welch's correction).

(D, E) Motor function assessment. Quantification of latency to fall in the rotarod test (D), alongside traverse time and the number of paw slips in the beam walking test (E), showing that ERK hyperactivation (*MEK1DD*) significantly rescues fine motor coordination deficits induced by LPC.

(F, G) Cognitive and memory function assessment. Quantification of spontaneous alteration in the Y-maze test (F) and the discrimination index and ratio in the novel object recognition test (NORT) (G), indicating that enhanced ERK signaling significantly ameliorates LPC-induced spatial working memory and recognition memory impairments. ($n \geqslant 12$ per group; mean ± SEM; one-way ANOVA followed by Tukey-Kramer post-hoc test).

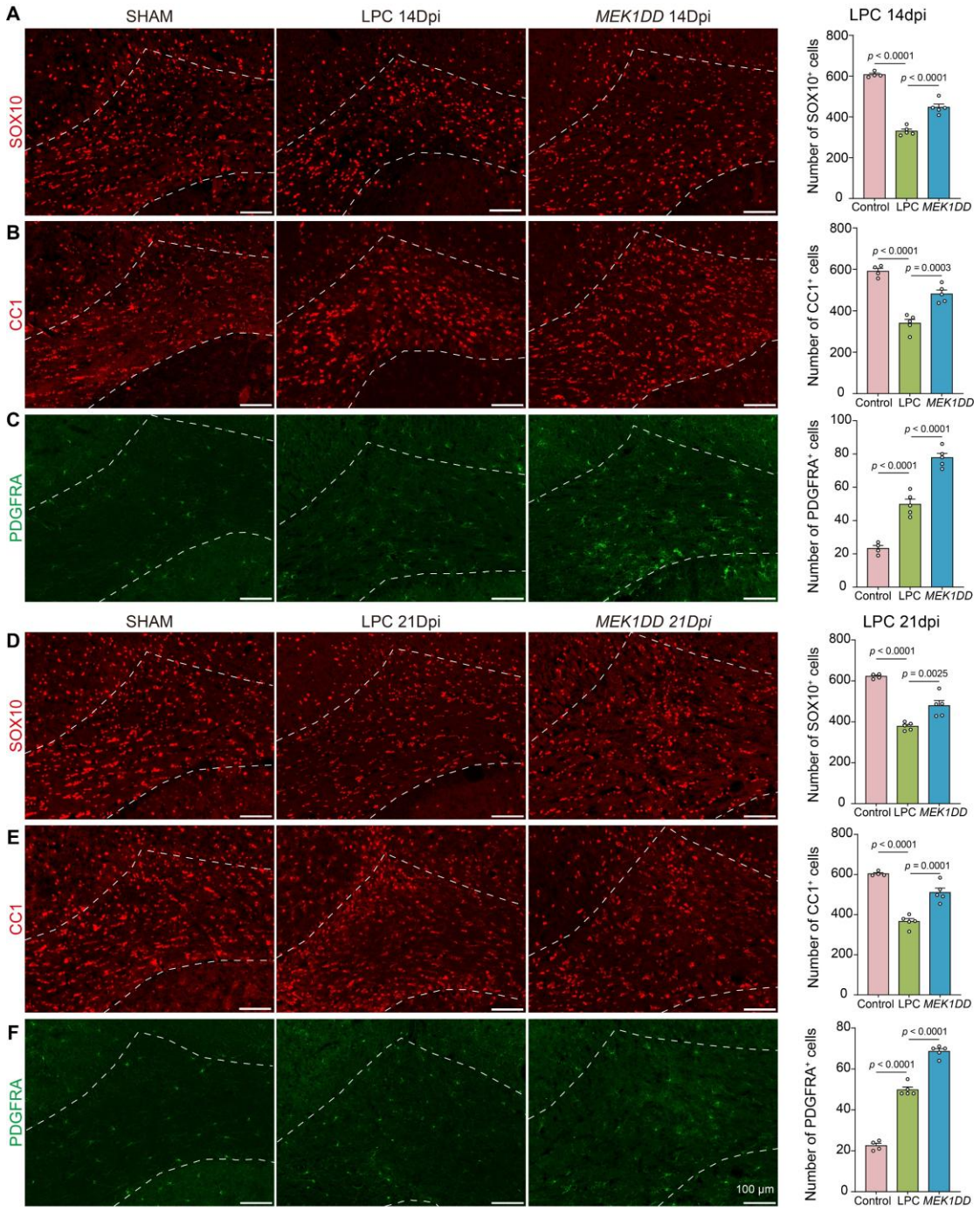

Figure 4. Enhanced ERK signaling drives the expansion and differentiation of oligodendrocyte lineage cells during remyelination.

(A–C) Representative immunofluorescence images and corresponding quantification of SOX10⁺ total oligodendrocyte lineage cells (A), CC1⁺ mature oligodendrocytes (B), and PDGFRA⁺ oligodendrocyte precursor cells (OPCs) (C) in the corpus callosum at 14 days post-injection (dpi). Compared to the LPC control group, the ERK-overexpressing group (*MEK1DD*) exhibits a significant increase in the numbers of all three cell populations.

(D–F) Representative images and quantification of SOX10⁺ (D), CC1⁺ (E), and

PDGFRA^{+} (F) cells in the corpus callosum at 21 dpi. Sustained ERK hyperactivation (*MEK1DD*) significantly elevates the generation of OPCs and their subsequent differentiation into mature oligodendrocytes relative to the LPC control group, providing a robust cellular basis for myelin repair. (n = 5 per group; mean ± SEM; one-way ANOVA followed by Tukey-Kramer post-hoc test).

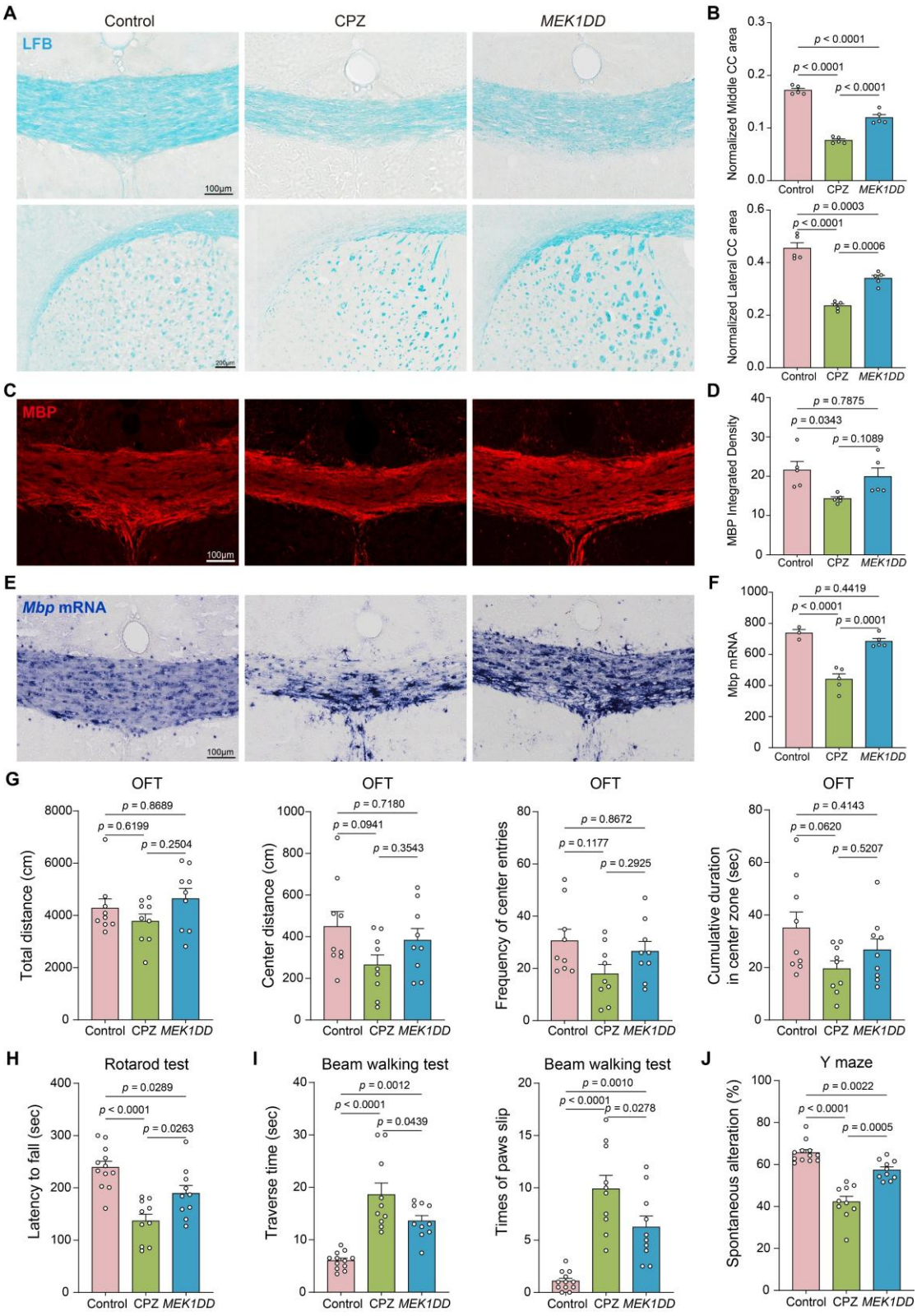

Figure 5. Enhanced ERK signaling promotes myelin repair and functional recovery in the CPZ-induced demyelination model.

(A, B) Representative Luxol Fast Blue (LFB) staining images (A) and quantification of

the normalized middle and lateral corpus callosum (CC) area (B). Compared to the CPZ control group, the ERK-overexpressing group (*MEK1DD*) exhibits a significantly preserved myelinated area.

(C–F) Representative images and quantification of MBP immunofluorescence (C, D) and *Mbp* mRNA *in situ* hybridization (E, F) in the corpus callosum. Enhanced ERK signaling robustly rescues *Mbp* transcriptional levels (F) and promotes the recovery of MBP protein expression (D) following CPZ-induced demyelination. ($n \geqslant 3$ per group; mean $\pm$ SEM; one-way ANOVA followed by Tukey-Kramer post-hoc test).

(G) Open field test (OFT) assessment. Quantification of total distance, center distance, frequency of center entries, and cumulative duration in the center zone shows comparable baseline locomotion and anxiety-like behaviors across all groups.

(H–J) Motor and cognitive function assessments. Quantification of latency to fall in the rotarod test **(H)**, traverse time and paw slips in the beam walking test **(I)**, and spontaneous alteration in the Y-maze test **(J)**. ERK hyperactivation ameliorates CPZ-induced fine motor coordination impairments and spatial working memory deficits. (n ≥ 9 per group; mean ± SEM; one-way ANOVA followed by Tukey-Kramer post-hoc test).

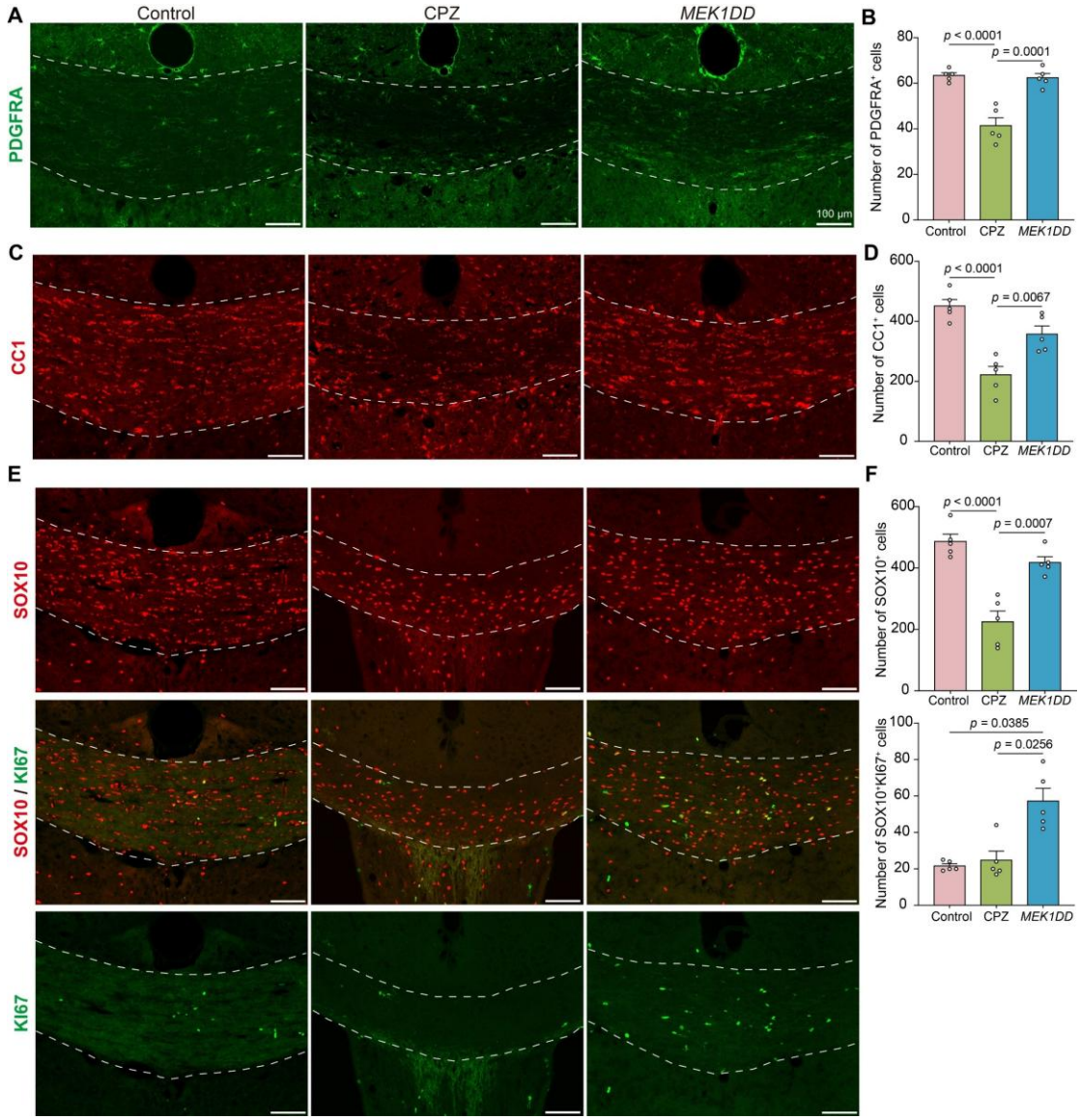

Figure 6. Enhanced ERK signaling drives the proliferation and repopulation of oligodendrocyte lineage cells following CPZ-induced demyelination. (A, B) Representative images (A) and quantification (B) of PDGFRA$^+$ oligodendrocyte precursor cells (OPCs).

(C, D) Representative images (C) and quantification (D) of CC1$^+$ mature oligodendrocytes in the corpus callosum. Sustained ERK hyperactivation significantly rescues the number of mature oligodendrocytes depleted by CPZ treatment.

(E, F) Representative immunofluorescence images (E) and corresponding quantification (F) of SOX10$^+$ total oligodendrocyte lineage cells and SOX10$^+$/KI67$^+$ proliferating oligodendrocyte lineage cells in the corpus callosum. Compared to the CPZ control group, the ERK-overexpressing group (*MEK1DD*) exhibits a significant restoration of the SOX10$^+$ cell pool, which is driven by a robust increase in cellular proliferation (SOX10$^+$/KI67$^+$ cells). (n = 5 per group; mean $\pm$ SEM; one-way ANOVA followed by Tukey-Kramer post-hoc test).

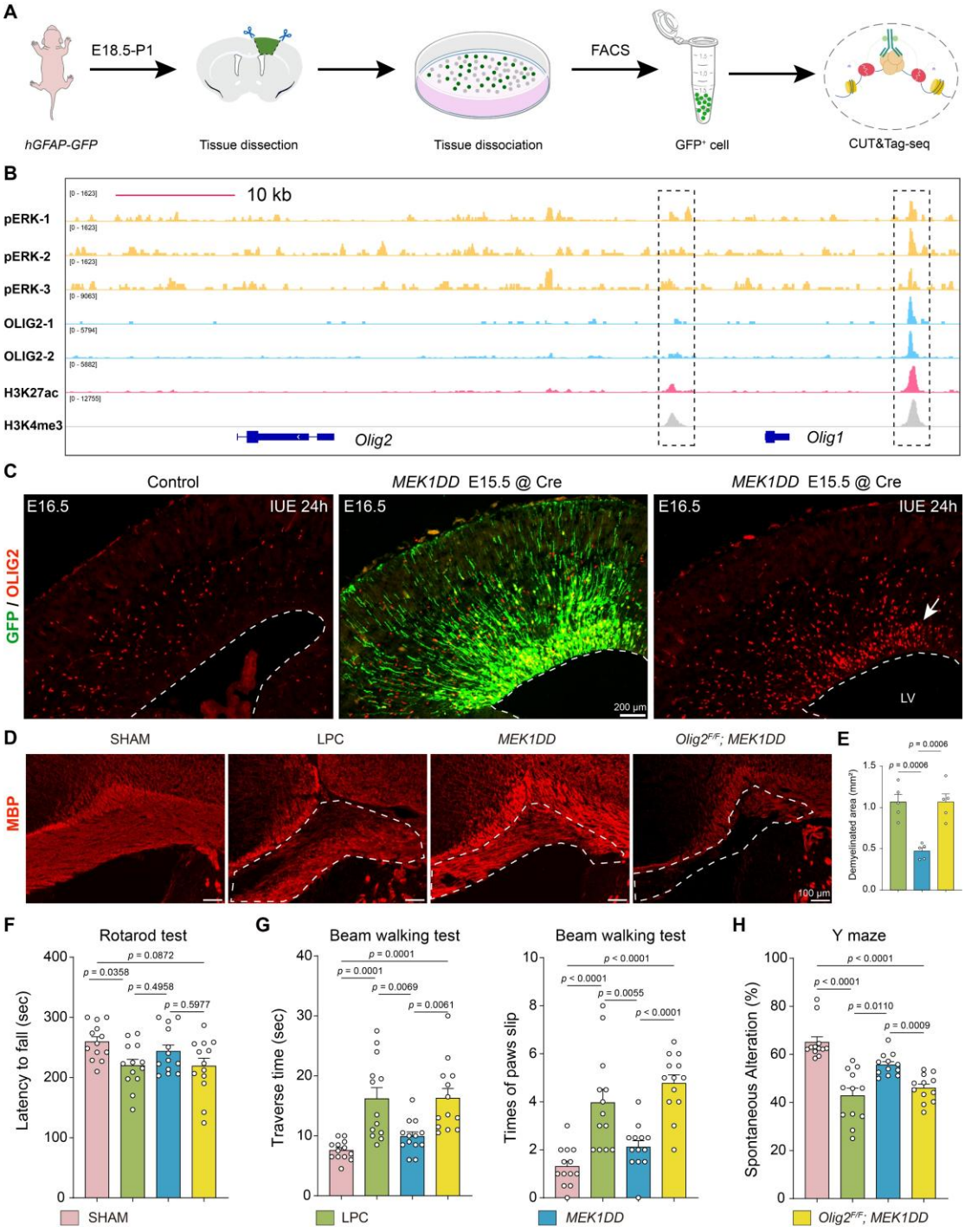

Figure 7. ERK directly targets *Olig2* to mediate oligodendrocyte lineage progression and myelin repair.

(A, B) Schematic workflow of CUT&Tag-seq using FACS-sorted GFP⁺ cells (A) and representative genome browser tracks (B). CUT&Tag analysis reveals distinct binding peaks of phosphorylated ERK (pERK) at the regulatory regions of the *Olig1* and *Olig2* loci, which co-localize with active chromatin marks (H3K27ac and H3K4me3).

(C) Representative immunofluorescence images of the cortex at E16.5 following *in utero* electroporation (IUE) at E15.5. Within just 24 hours post-electroporation, ERK hyperactivation (*MEK1DD*) induces a massive and rapid upregulation of OLIG2 expression in the electroporated cells compared to the control, validating *Olig2* as a direct downstream target of ERK.

(D, E) Representative MBP staining images (D) and quantification of the demyelinated area (E) in the focal LPC model. The robust remyelination-promoting effect of ERK hyperactivation (*MEK1DD*) is significantly abolished upon the concurrent conditional knockout of *Olig2* (*Olig2*$^{F/F}$*; MEK1DD*). (n = 5 per group; mean ± SEM; one-way ANOVA followed by Tukey-Kramer post-hoc test).

(F–H) Behavioral assessments including the rotarod test (F), beam walking test (G), and Y-maze test (H). The significant functional recovery in motor and cognitive performance achieved by *MEK1DD* is effectively reversed by the deletion of *Olig2*, demonstrating that OLIG2 is functionally indispensable for ERK-mediated myelin repair. (n ⩾ 12 per group; mean ± SEM; one-way ANOVA followed by Tukey-Kramer post-hoc test).

Supplementary Files

This is a list of supplementary files associated with this preprint. Click to download.

- SupplementaryMaterials.docx